In the *Proceedings of the International Symposium on Visual Computing (ISVC)*, 2011

Free Boundary Conditions Active Contours with Applications for Vision

Michal Shemesh and Ohad Ben-Shahar
shemeshm,ben-shahar@cs.bgu.ac.il

Ben-Gurion University of the Negev, Beer-Sheva, Israel

Abstract. Active contours are used extensively in vision for more than two decades, primarily for applications such as image segmentation and object detection. The vast majority of active contours models make use of *closed* curves and the few that employ open curves rely on either fixed boundary conditions or no boundary conditions at all. In this paper we discuss a new class of open active contours with *free boundary conditions*, in which the end points of the open active curve are restricted to lie on two parametric *boundary* curves. We discuss how this class of curves may assist and facilitate various vision applications and we demonstrate its utility in applications such as boundary detection, feature tracking, and seam carving.

1 Introduction

Active contours (a.k.a. snakes) is a popular family of models in which each possible contour $C(s)$ in the image plane is associated with an energy, and once initialized (manually or automatically), the contour deforms continuously in order to converge to an optimal energetic state. Suggested first by Kass *et al.* [1], the original formulation of active contours uses an explicit parametric representation of the curve and therefore became known as the *parametric active contour model*. The energy of active contours is usually formulated as a functional containing an internal and external energy terms

$$E_{curve}(C(s)) = \int [E_{int}(C(s)) + E_{ext}(C(s))]\, ds\ . \tag{1}$$

During the evolution of the contour, the internal energy term controls its shape while the external energy term attracts the curve to certain image features. One can define each of them according to the desired applications, which typically have been either linear features detection (e.g. [2–4]), image segmentation (e.g. [5, 6]), object detection (e.g. [7, 8]), or motion tracking (e.g. [9–11]). Owing to the type of applications that they have been usually adopted for, most existing active contour models are formulated on *closed* curves, while much fewer *open* active models are put to use. Interestingly, however, the first instance of open active contours (OAC) was already presented in the seminal work by Kass *et al.* [1], and since then it has been adapted occasionally for applications that involve

linear features, for example in geophysical [3], medical [12], or biological [4, 13] contexts. Apart from distinct energy functionals that suit their respective applications, the different uses of OAC have been characterized by their different boundary conditions. Notably, these different boundary conditions have focused exclusively on two cases: either *fixed boundary conditions* or *no boundary conditions* at all. In this work we present and formulate a third class of OACs, whose boundary conditions are known in the calculus of variations as "*free*" [14, pp. 68-74]. We discuss why this type of objects is potentially a most useful class of active contours for vision and we demonstrate it in the context of several different applications.

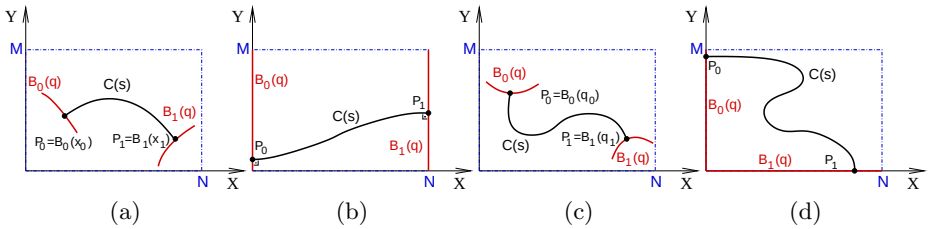

Fig. 1. Four typical examples for OAC (black) and boundary curves (red) drawn on an image I. An OAC which is represented as a function of one variable (a-b) and as a parametric curve (c-d).

2 Related Work

As mentioned above, OAC have been used much less frequently in vision, and when they are employed it is either with fixed boundary conditions or no boundary conditions at all. Fixed boundary conditions, the case where both end points of the active contour are fixed in space, were used for linear feature detection in road maps and medical images [12, 15–17]. In such cases, the end points are assumed to be anchors that are known with full certainty in advance and hence need not shift in space during evolution. This situation reflects the most fundamental minimization problem of calculus of variation (i.e., the problem of finding the shortest string between two given end points [18, pp. 33-34]) and in practice it involves a curve evolution that resembles the classical closed snake for all points except at the end points (which preserve their position throughout the iterations). Unlike this classical problem, visual OAC with fixed boundary conditions also involve the influence of external forces.

Once the initial curve is set with its two end points fixed in place, additional "inflation" [12] or "deflation" [17] forces can reduce its sensitivity to local minima during the evolution. Alternatively, local minima have been handled by global search via dynamic programming. Such approach was first implemented for the active contours parametric model [19] and later on used to find the path

of minimal cost between two given points using either the surface of minimal action [15] or a function describing at each point the minimal cost of a curve connecting that point to a pre-determined "source point" in the image [16].

In some application, where the desired end points of the snake are not known a priori, fixed boundary conditions are clearly improper. In such cases, the energy of the OAC is endowed with "stretching forces" that affect its end points in the direction tangent to the curve [4]. Related also to earlier ideas on incremental "snake growing" [2, 20], this approach assumes no special constraints on the end points, and hence evolves all snake points similarly. In cases where the movement of the end points is not only in the tangential direction, internal energies such as inertia and differential energy are integrated [10] and affect the movement of the end points as well.

While open curves are more naturally represented parametrically, OAC have also been considered implicitly [21] in the spirit of modern approaches to active contours that employ level set formulations (e.g., [22–24]). Since OAC are naturally suited for linear features like edges and filaments, they are less consistent with the fact that level sets of functions are generically closed curves. Hence, an implicit representation for OACs was suggested via the medial axis-derived centerline of a level set function induced by the curve [21]. To fit better the closed nature of levelsets, an alternative approach defined the OAC via functions whose levelsets partially surround the image margins but cross its interior along a linear feature of interest [25]. This solution, however, is appropriate only when the open curve connects two different margins of the image, which is usually not the case. Here too the end points obey no boundary condition behavior in order to stretch along the sought-after linear features.

Since OAC are naturally suited for thin and elongated features, applications of both types of OAC models have focused on those cases where one needs to detect such features more robustly than local edge detection can provide. Included among such application are the extraction of roads (e.g., [10, 16, 21]), the detection of coastlines in satellite images (e.g., [3]), model-based contour detection (e.g., [26, 27]), extraction of thin linear features in medical or biological contexts (e.g., [4, 12, 13, 16]), and boundary detection (e.g., [2, 17]).

Unlike the previous types of OAC, in this paper we propose a new class of OAC with *free boundary conditions*. In this model each of the two end points of the OAC is free to move, but it is entitled to do so in a very particular and constrained fashion, namely along a given parametric *boundary* curve, as shown in Fig. 1 (red). This configuration is often natural in vision applications, where it is known a priori that the end points cannot depart from a particular image plane structure of co-dimension 1. Furthermore, this formulation can greatly simplify the initialization process of active contours by providing *some* freedom for the initial location of the end points (unlike in "fixed boundary conditions" case) but not *too much* freedom (as in the "no boundary conditions" case) that can divert the final convergence state of the snake from the desired location. In the rest of this paper we first discuss the mathematical principles that drives this class of

OAC and then describe and demonstrate its practicality for applications ranging from boundary detection and recognition, through tracking, to seam carving.

3 Mathematical Foundations

Active contours are deformable curves in images which evolve over time to an optimal energetic state. The energy functional from Eq. 1 can be expressed more explicitly by

$$E_{curve} = \int_0^1 \left[f(C, C', \ldots) + g(I(C), \frac{\partial I}{\partial x}(C), \frac{\partial I}{\partial y}(C), \ldots) \right] ds \tag{2}$$

where $C(s) : [0,1] \rightarrow \Re^2$ describes a parametrized differentiable planar curve in an image $I : [0,M] \times [0,N] \rightarrow \Re$, $f(\cdot)$ is a function of the curve, and $g(\cdot)$ is a function of the image beneath the curve (including their derivatives up to some desired order). During the evolution of the active contour toward minimal energetic state, the $f(\cdot)$ function controls its shape while the $g(\cdot)$ function pulls the curve to certain image features. In the classical snakes by Kass *et al.* [1], the active contour energy functional was defined as follows

$$\begin{array}{c} E_{curve} = \int_0^1 \left[\alpha |C'(s)|^2 + \beta |C''(s)|^2 + g(s) \right] ds \\ g(s) = -\gamma \left| \nabla (G_\sigma * I(C(s))) \right| \ , \end{array} \tag{3}$$

where α and β control the elasticity and rigidity of the contour, respectively, γ weighs in the degree to which high gradient regions attract it, and G_σ is a smoothing Gaussian kernel with standard deviation σ.

In contrast to fixed or no boundary conditions used for open active contours, in the OAC framework discussed here, the end points of our OAC open curve are restricted to lie on two parametric *boundary* curves. This type of *free boundary conditions* requires special care in the control of end point dynamic, as dictated by the calculus of variations [14, 28] and derived below in the next subsections.

Before we turn to derive the dynamics of OAC and the constraints induced by the free boundary conditions, we note that an OAC in the image plane can be represented in various ways. Most generally, it can be represented as a parametric curve $C(s) = (x(s), y(s))$, and the analysis for this case is presented in the next subsection. However, if the OAC is stretched "left to right" in the image plane and is not allowed to "backtrack" at any point then it may be represented more simply as a function of the form $y = y(x)$ (i.e, $C(s) = (s, y(s))$ (See Fig. 1a,b). In such cases, the variational analysis becomes univariate and provides additional insights, but since it is a special case of the general analysis, it is derived in the Supplementary Materials only.

3.1 The Variational Problem for $C(s) = (x(s), y(s))$

Assume one represents the OAC as a generalized parametric representation of the OAC as $C(s) = (x(s), y(s))$, where s is the curve parameter. For simplicity, suppose again that the energy functional over the curve is limited to first order

derivatives. Under these assumptions the energy functional from Eq. 3 can be written generally as

$$J[C(s)] = \int_0^1 \Phi(x, y, x', y')ds \ , \tag{4}$$

where Φ incorporates both the internal and external terms. Suppose now that the two end points of the active contour, i.e, $P_0 \stackrel{\triangle}{=} C(0)$ and $P_1 \stackrel{\triangle}{=} C(1)$ are constrained to lie on two smooth boundary curves $B_0(q)$ and $B_1(q)$, respectively, where $B_i(q) : [0,1] \rightarrow \Re^2$ $(i = 0, 1)$. Let q_0 and q_1 be the parameter values, where $C(s)$ intersects the boundary curves $B_0(q)$ and $B_1(q)$, i.e.,

$$\begin{array}{ll} B_0(q) = (X_0(q), Y_0(q)) & P_0 = C(0) = B_0(q_0) \\ B_1(q) = (X_1(q), Y_1(q)) & P_1 = C(1) = B_1(q_1) \end{array} \ , \tag{5}$$

as illustrated in Fig. 1c. This free boundary variational problem leads to the following *coupled* pair of Euler-Lagrange equations [14, 28]

$$\begin{array}{l} \Phi_x - \frac{d}{ds}\Phi_{x'} = 0 \\ \Phi_y - \frac{d}{ds}\Phi_{y'} = 0 \end{array} \ . \tag{6}$$

The additional end point constraints now become (see [14, pp. 222-228])

$$\begin{array}{l} (\Phi_{x'}, \Phi_{y'})|_{s=0} \cdot (X_0', Y_0')|_{q_0} = (\Phi_{x'}, \Phi_{y'})|_{s=0} \cdot B_0'|_{q_0} = 0 \\ (\Phi_{x'}, \Phi_{y'})|_{s=1} \cdot (X_1', Y_1')|_{q_1} = (\Phi_{x'}, \Phi_{y'})|_{s=1} \cdot B_1'|_{q_1} = 0 \end{array} \tag{7}$$

(where $\Phi_{x'}$, $\Phi_{y'}$ stands for $\Phi_{x'}(x, y, x', y')$ and $\Phi_{y'}(x, y, x', y')$, respectively). These constraints imply a particular geometrical configuration at the two end points. We observe that the vector of partial derivatives of the function Φ with respect to x' and y' should be perpendicular to the curves B_0, B_1 at the end points P_0, P_1, respectively. This constraint is typical of variational problems with free boundary conditions and is known as the *transversality conditions* (see [14, pp. 72-73]).

3.2 Implementation for a typical visual OAC

Let the OAC be represented as a general parametric curve $C(s)$ and let us consider an energy function Φ from the family described in Eq. 3. For simplicity of presentation, in the following we will also assume $\beta = 0$ (see the Supplementary Materials for the more general case) and hence, applying Eq. 6 on the functional

$$E_{curve} = \int_0^1 \left[\alpha |C'(s)|^2 + g(s)\right] ds \ \ , \ \ g(s) = -\gamma \left|\nabla (G_\sigma * I(C(s)))\right| \ , \tag{8}$$

yields the following two Euler-Lagrange equations

$$\begin{array}{lll} \Phi_x - \frac{d}{ds}\Phi_{x'} = 0 & \Rightarrow & -2\alpha x'' + \frac{\partial}{\partial x} g = 0 \\ \Phi_x - \frac{d}{ds}\Phi_{y'} = 0 & \Rightarrow & -2\alpha y'' + \frac{\partial}{\partial y} g = 0 \ . \end{array} \tag{9}$$

One more thing we need to take care of is the specific form that the transversality constraint takes for our selected energy functional. Applying Eq. 7 to our specific Φ functions yields the following additional end point constraints

$$\begin{array}{l} 2\alpha\ (x',y')|_{s=0} \cdot (X_0', Y_0')|_{q_0} = 0 \\ 2\alpha\ (x',y')|_{s=1} \cdot (X_1', Y_1')|_{q_1} = 0\ . \end{array} \tag{10}$$

Note that in this particular case the transversality constraint implies that the OAC must remain *orthogonal* to the boundary curves on both ends.

While the necessary conditions expressed in Eq. 9 should be satisfied at the extrema points of the functional, a standard way to obtain these extrema is to use these equations in a steepest descend fashion [2, 3, 1]. Hence, if $C(s,t)$ represents the curve $C(s)$ at time t, its evolution over time is given by

$$C_t(s,t) \triangleq \frac{\partial}{\partial t} C(s,t) = -2\alpha C''(s,t) + \nabla g(s,t)\ . \tag{11}$$

Obviously, should any particular application require or desire a different composition of internal and external energies (cf. Eqs. 1 through 8), the Euler-Lagrange and the dynamics of the OAC would need to adjust accordingly.

In practice, the OAC is represented as a time-evolving series of *control points* $\{x_i^t, y_i^t\}$ for $i = 1...n$. In order to enforce boundary conditions in each time step in the OAC's evolution in a way that respects Eq. 10, one must adjust the end points (points 1 and n) such that (1) they remain on the boundary curves and (2) the boundary curves are perpendicular to the OAC. More explicitly, the new coordinates for point $i = 1$ (P_0) which should be placed on boundary curve B_0 (see Fig 1 and Eqs. 5) are $P_0 = (X_0(q_0), Y_0(q_0))$ when q_0 is the root of the polynomial $D(q)$ (representing the derivative of the distance between point $i = 2$ of the OAC and the curve B_0)

$$D(q) = ((X_0(q) - x_2)X_0^{'}) + ((Y_0(q) - y_2)Y_0^{'})\ , \tag{12}$$

s.t. $0 \leq q_0 \leq 1$. The computation for the new coordinates of point $i = n$ is analogous. A detailed presentation of additional mathematical derivations and numerical considerations is presented in the Supplementary Material.

3.3 Properties of the dynamics

At first sight it seems that the difference between OACs with and without free boundary conditions are negligible as the only operational differences between them is the application of transversality. It remains to discuss how critical is this constraints is in practice, and how it affects the dynamics of the OAC. In this context two comments are in order.

Intuitively, when internal forces are missing, one would expect the end points to remain on the boundary curves while obeying external forces only. Indeed, when $\alpha = 0$ we get $(\Phi_{x'}, \Phi_{y'}) = (0,0)$, transversality as expressed in Eq. 7 becomes meaningless, and the OAC would evolve under the influence of external forces only. On the other hand, when only internal forces control the curve, transversality constraints become an operational *necessity*.

Since the application of transversality is operational important, it remains to discuss how this reconciles with the fact that not always an object boundary or other linear features will be perpendicular to the boundary curve. Indeed, as

most regularizations prevents classical active contours from accurately locking on sharp features like corners, so does transversality in OAC with free boundary conditions, which might entail a slight deviation from the genuine image-based feature where it meets the boundary curve. In practice, the advantages of OAC with free boundary conditions well exceed this limitation since the the deviation extends no more than one pixel from the boundary curves and hence virtually unnoticeable.

4 Applications for Vision

OAC with free boundary conditions offer a new platform for a number of applications. In this section we discuss several such applications and the benefits that are introduced by addressing them with our new type of OACs. We emphasize that at this point it is not our goal to claim that using OAC with free boundary conditions is necessarily better than traditional techniques that have been studied extensively in the context of these applications, nor do we attempt to exhibit better than state-of-the-art performance in any of these applications. Rather, in discussing these applications we hope to present the opportunities that could lie ahead in using this class of OAC. Clearly, to beat the state-of-the-art one would need to optimize the use of these objects for any particular application, and in particular, further research would be required in each case in order to select the energy functional and the choice of the free boundary conditions accordingly.

4.1 Boundary Detection

Boundary detection is one of the most natural and popular applications of active contours. As we now discuss, using OACs with free boundary conditions may be a better choice for certain instances of this application.

Consider for example the detection of coastlines in satellite images [3, 29, 25]. In most cases the end points of the curve describing the coastline reside on the image boundaries and the importance of their correct localization in these regions is no lesser than any other point of the coastline. Hence, using *fixed* boundary conditions is appropriate only if one is able to determine the location of these end points accurately in advance. On the other hand, setting *no* boundary conditions may result in uncompleted detection of the coastline in case the end points depart from the image margins in the course of the evolution. Since in our case it is known that the end points must lie on the image margins, one may set these margins as free boundary conditions, and allow the curve to localize the coastline end points on the image margins as part of the evolution process, as Fig 2 shows, this provides superior results which neither classical OAC can provide. The same figure shows the application of the same tool in agricultural setting, though here the boundary condition curves are defined inside the image. The initial contour evolves to lock down on the correct object contour and performs completion of the occluded areas. The external energy term was defined as $g = -\gamma \left|\nabla(G_\sigma * I(C))\right|$ with $\sigma = 2$.

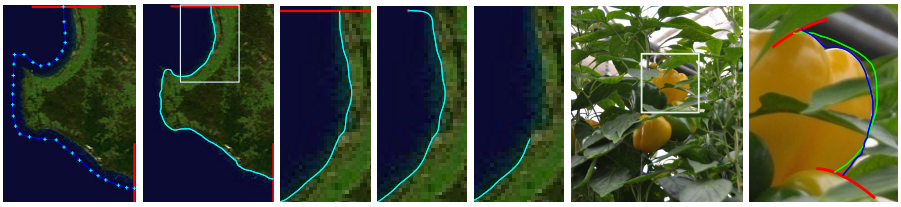

(a) (b) (c) (d) (e) (f) (g)

Fig. 2. A parametric OAC successfully locks down on linear features. The initial (a, shown via discrete control points), and final (b) convergence state of an OAC on a coastline satellite image ($\alpha = 0.5$, $\gamma = 2$). Boundary curves (red) coincide with the image margins. Closeup of the ROI in panel b, and results using *free* (c), *fixed* (d), and *no* (e) boundary constraints. Three corresponding videos are provided in the supplementary material. Panel f and the closeup in panel g show similar application in agricultural setting where The very rough initial contour (green) evolves to lock down on the correct object contour (blue). With proper definition of the external energy, this process can also completes the occluding contour of the fruit over the occluders.

Note that for the detection of linear features such as those discussed above, the setting of the boundary conditions requires less extra care or scrutiny as would be necessary with fixed boundary conditions. This represents a generic advantage of OAC with free boundary conditions – it allows the user to specify boundary conditions easily and quickly and be sure that the resulting curve will not escape these regions during the evolution of the curve. In practice, all that is requires is a curve that intersects the linear feature, rather than a point that sits exactly on it. As shown in Fig. 2, this provides better results than traditional OAC up to the effect of transversality as discussed in Sec. 3.3.

4.2 Feature Tracking

Active contours have been used successfully for tracking ever since their introduction to the vision community, and similar to their use for detection and segmentation, most tracking applications employ *closed* curves [30]. If the feature to be tracked is linear in structure, however, the natural active contour to use would be open. Still, since end points of linear features also tend to exhibit motion in video sequences (just imagine the margins of a road viewed from the driver's seat), the use of fixed boundary conditions becomes improper. In many cases, however, the end points are restricted to move along a known curve in the image plane, either because the linear feature slides along the image margins or along an occluder, or because of some known physical constraint in the world. In such cases, using OAC with free boundary conditions is the natural choice for insuring accurate tracking results.

One example is shown in Fig. 3 (upper row). Here the goal is to track the margins of the road, whose position changes from one frame to another. Since during the video sequence the road margins slide along the image margins, it

is possible to defined these boundaries (or parts of them) as the free boundary conditions of an OAC that tracks the road from frame to frame. The convergence state at each frame serves as the initial OAC for the next frame (in this case the first frame was initialized manually), which is then driven to its optimal state to lock again on the road margins. In this example external energy term was defined by the negative values of the image gradient, i.e., $g = -\gamma\,|\nabla(G_\sigma * I(C))|$ with $\sigma = 2$ in order to extend the attraction region of the curve to the road strips. Note how the free boundary conditions ensure that the road is tracked successfully along its full extent.

The additional tracking example shown in Fig. 3 (lower row) demonstrates a case where the boundary curves are determined by a physical constraint in the world. Here we seek to follow the rising spark in Jacob's ladder[1], which is formed between two static wires but is free to move along them. This configuration fits naturally the free boundary conditions setup, where the boundary curves are defined along the wires. The external energy was defined by the negative value of the gray level image intensity, i.e., $g = 1 - |(G_\sigma * I(C))|$ ($\sigma = 2$) in order to attract the curve to the bright spark. Note that tracking configurations like this are prevalent in natural scenarios, and include traveling waves between walls, behavior of soap films, constrained viscous fluid dynamics, and more.

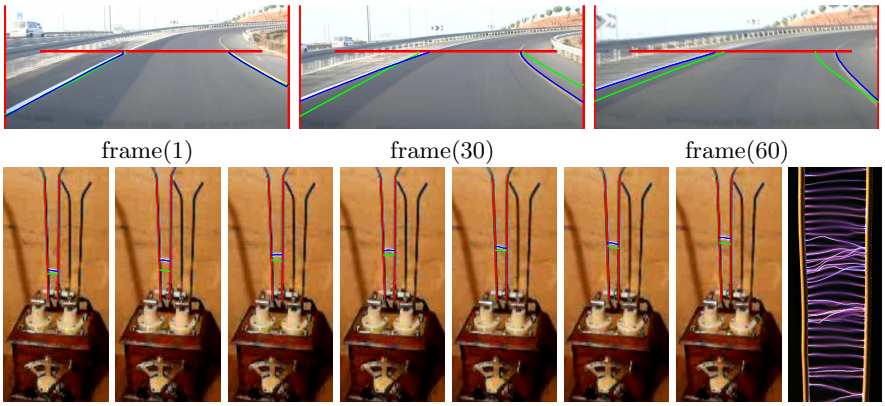

Fig. 3. Upper row: Road extraction and tracking using two OACs ($\alpha = 2$, $\gamma = 1$). Superimposed on each frame are the initial and final OACs configurations (in green and blue, respectively). The green OACs in frames 30 and 60 are the final OAC from the previous panels (frames 1 and 30, respectively). and the free boundary conditions are set to the red curves. A video is provided in the supplementary material. **Lower row:** The rising spark in Jacob's ladder ($\alpha = 0.1$, $\gamma = 1$) (right, showing time exposures of the phenomenon) The images show seven consecutive frames, each showing the initial and final configurations (in green and blue, respectively) Boundary curves (red) were aligned with the wires in all frames.

[1] Jacob's ladder is a device for producing a continuous train of sparks which rise upwards. The spark gap is formed by two wires, approximately vertical but gradually diverging away from each other towards the top in a narrow "V" shape.

4.3 Seam Carving

Seam carving [31, 32] is a popular approach for content-aware image resizing. In this method the image size and aspect ratio are changed by repeatedly removing or inserting low energy paths of pixels called *seams*. While seam carving employs discrete methods for finding optimal seams, a natural alternative is using the continuous framework of OAC with free boundary conditions. In this case, instead of a monotonic and connected path of low energy pixels crossing the image from left to right (or top to bottom), representing seams as OAC with free boundary conditions provides the opportunity to consider them in a continuous domain, where image boundaries define the free boundary conditions between which the curves are stretched (as shown in Figs. 1b and 4 (red) and defined in Sec. 4.1).

The use of OAC for image resizing using seam carving can be performed with the following steps in a repeated fashion. First, an initial contour connecting opposite margins of the image is selected, either arbitrarily or using a more informative selection process. Then the OAC evolves until a minimal energetic configuration is found while the proper pair of image boundaries serve as free boundary conditions curves. Finally, the parametric OAC is converted into a set of pixels for removal or insertion. The flexibility of the OAC framework allows to define each one of these operations in one of many ways according to the desired application of interest.

Although using OAC with free boundary conditions for seem carving deserves a research program in its own right, it is clear that representing seams as such OAC could carry many advantages over the traditional discrete representation used thus far. First, they facilitates much larger space of optimal seams, since OAC are not restricted to maintain monotonicity as opposed to the traditional seam definition. For the same reason, such OAC are not restricted to a $[-45°, 45°]$ sector, as dictated by monotonicity in a regular pixel grid. Furthermore, these objects allow for easy incorporation of geometrical constraints in addition to image-based criteria and they readily facilitate super resolution seam carving by their very continuous nature.

Fig. 4 shows two examples of seam carving using OAC with free boundary conditions. In this example, each initial contour was set as a traditional optimal seam and then evolved to minimal energetic state. Then, all l_i pixels that intersect the OAC in row i of the image were replaced with $l_i - 1$ pixels by averaging the color of each two neighboring pixels into one. In this case, we used $\alpha = 0.05$, $\gamma = 1$, and $\sigma = 1$ and the external energy was defined as $-g$ from Eq. 8 in order to attract the contour towards homogeneous areas.

5 Summary

We presented and discussed a new class of open active contours with *free boundary conditions*, in which the end points of the open active curve are restricted to lie on two parametric *boundary curves* in the image plane. Being continuous and detached from the discrete and regular structure of the pixel array, these

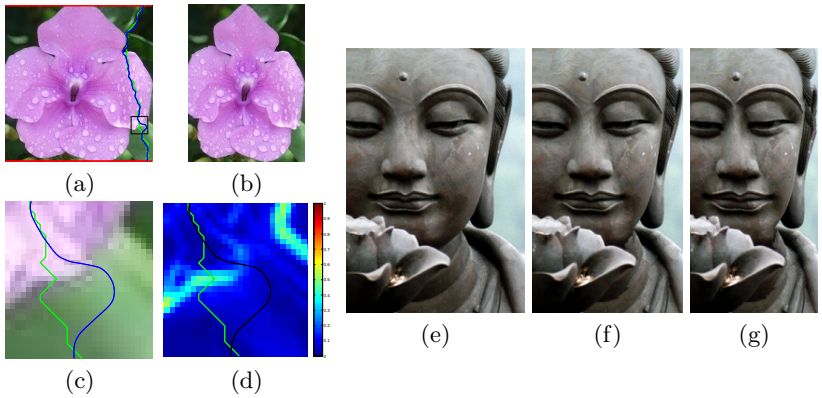

Fig. 4. (a) An initial OAC (green) and the final convergence configuration (blue). **(b)** A result of seam carving using OAC applied for 50 iterations. **(c)** A closeup of the region of interest from panel a shows the dramatic change in the seam that occurred during the evolution from the traditional seam to the minimal energy OAC. **(d)** Same two close up seams, shown on the energy map of the image, and explain why the OAC elected to evolve to this final result.**(e-g)** An original image and the result of carving out 30 and 55 vertical seams using OAC.

objects facilitate the extension of several applications in vision, they simplify the initialization procedure, and they provide a natural framework for sub pixel computation in the context of many applications.

Acknowledgments: This work was funded in part by the European Commission in the 7th Framework Programme (CROPS GA no 246252). We also thank the generous support of the Frankel fund and the Paul Ivanier center for Robotics Research at Ben-Gurion University.

References

1. Kass, M., Witkin, A., Trezopoulos: Snakes: Active contour models. Int. J. Comput. Vision **1** (1988) 321–331
2. Berger, M.O., Mohr, R.: Towards autonomy in active contour models. In: ICPR. Volume 1. (1990) 847–851
3. Della Rocca, M.R., Fiani, M., Fortunato, A., P.Pistillo: Active contour model to detect linear features in satellite images. Int. Arch. Photo. Remote Sens. Spat. Inf. Sci. **34** (2004)
4. Li, H., Shen, T., Smith, M.B., Fujiwara, I., Vavylonis, D., Huang, X.: Automated actin filament segmentation, tracking and tip elongation measurements based on open active contour models. IEEE Int. Symp. on Biomed. Imaging **15** (2009)
5. Williams, D.J., Shah, M.: A fast algorithm for active contours and curvature estimation. CVGIP **55** (1992)
6. Basu, S., Mukherjee, D.P., Acton, S.T.: Active contours and their utilization at image segmentation. In: Proceedings of Slovakian-Hungarian Joint Symposium on Applied Machine Intelligence and Informatics Poprad. (2007) 313–317

7. Velasco, F.A., Marroquin, J.L.: Robust parametric active contours: the sandwich snakes. Machine Vision and Applications (2001) 238–242
8. Xu, C., Prince, J.: Snakes, shapes, and gradient vector flow. IEEE Trans. Image Processing **7** (1998) 359–369
9. Leymarie, F., Levine, M.D.: Tracking deformable objects in the plane using active contour model. IEEE Trans. Pattern Anal. Mach. Intell. **15** (1993)
10. Sawano, H., Okada, M.: Road extraction by snake with inertia and differential features. In: ICPR. Volume 4. (2004) 380–383
11. Srikrishnan, V., Chaudhuri, S.: Stabilization of parametric active contours using a tangential redistribution term. IEEE Trans. Image Processing **18** (2009) 1859–1872
12. Cohen, L.D.: On active contour models and balloons. CVGIP **53** (1991) 221–218
13. Saban, M.A., Altinok, A., Peck, A.J., Kenney, C.S., Feinstein, S.C., Wilson, L., Rose, K., Manjunath, B.S.: Automated tracking and modeling of microtubule dynamics. IEEE Int. Symp. on Biomed. Imaging (2006) 1032–1035
14. Sagan, H.: Introduction to the Calculus of Variations. McGraw-Hill, Inc. (1969)
15. Cohen, L.D., Kimmel, R.: Global minimum for active contour models: A minimal path approach. Int. J. Comput. Vision **24** (1999) 57–78
16. Melonakos, J., Pichon, E., Angenent, S., Tannenbaum, A.: Finsler active contours. IEEE Trans. Pattern Anal. Mach. Intell. **30** (2008) 412–23
17. Gunn, S.R., Nixon, M.S.: Global and local active contours for head boundary extraction. Int. J. Comput. Vision **30** (1998) 43–54
18. van Brunt, B.: The Calculus of Variations. Springer-Verlag New York inc. (2004)
19. Amini, A., Tehrani, S., Weymouth, T.: Using dynamic programming for minimizing the energy of active contours in the presence of hard constraints. In: ICCV. (1988) 95–99
20. Velasco, F.A., Marroquin, J.L.: Growing snakes: active contours for complex topologies. Pattern Recognition **36** (2003) 475–482
21. Basu, S., Mukherjee, D.P., Acton, S.T.: Implicit evolution of open ended curves. In: ICIP. (2007) I: 261–264
22. Caselles, V., Catte, F., Coll, T., Dibos, F.: A geometric model for active contours in image processing. Numerische Mathematik **66** (1993) 1–31
23. Malladi, R., Sethian, J.A., Vemuri, B.C.: Shape modeling with front propagation: a level set approach. IEEE Trans. Pattern Anal. Mach. Intell. **17** (1995) 158–175
24. Caselles, V., Kimmel, R., Sapiro, G.: Geodesic active contours. Int. J. Comput. Vision **22** (1995) 61–79
25. Cerimele, M.M., Cinque, L., Cossu, R., Galiffa, R.: Coastline detection from SAR images by level set model. In: CAIP. (2009) 364–373
26. Fua, P., Leclerc, Y.G.: Model driven edge detection. Machine Vision and Applications **3** (1990) 45–56
27. Kimmel, R., Bruckstein, A.: Regularized laplacian zero crossing as optimal edge integrators. Int. J. Comput. Vision **53** (2003) 225–243
28. Gelfand, I., Fomin, S.: Calculus of Variations. Prentice-Hall, Inc. (1963)
29. Lesage, F., Ganon, L.: Experimenting level-set based snakes for contour segmentation in radar imagery. In: Proc. of the SPIE. Volume 4041. (2000) 154–162
30. Blake, A., Isard, M.: Active Contours: The Application of Techniques from Graphics, Vision, Control Theory and Statistics to Visual Tracking of Shapes in Motion, 1st edition. Springer-Verlag New York, Inc. (1998)
31. Avidan, S., Shamir, A.: Seam carving for content-aware image resizing. ACM Trans. Graph. **26** (2007) 10
32. Rubinstein, M., Shamir, A., Avidan, S.: Improved seam carving for video retargeting. ACM Trans. Graph. **27** (2008) 1–9